JOURNAL OF SOLID STATE CHEMISTRY **131,** 275–281 (1997)
ARTICLE NO. SC977375

Metal–Semiconductor Transition of $La_2NiO_{4+\delta}$

K. Ishikawa,[1] W. Shibata, K. Watanabe, T. Isonaga, M. Hashimoto, and Y. Suzuki

Department of Industrial Chemistry, Faculty of Engineering, Meiji University, Higashi-mita, Tama-ku, Kawasaki 214, Japan

Received August 19, 1996; in revised form March 4, 1997; accepted March 5, 1997

The excess oxygen concentrations of $La_2NiO_{4+\delta}$ have been measured in 0.00–6.06, 13.33–18.25, or 66.66–71.40 kPa of oxygen in the range 300–1273 K by the desorption method. The electrical conductivities of $La_2NiO_{4+\delta}$ have been also measured in 1.33, 13.33, 66.66, or 101.33 kPa of oxygen in the range 77.4–1273 K or under a helium atmosphere (1 atm) in the range 77.4–300 K. The mechanism of the metal–semiconductor transition of $La_2NiO_{4+\delta}$ is discussed on the basis of the excess oxygen concentration and the electrical conductivity data. The metal–semiconductor transition of $La_2NiO_{4+\delta}$ is explained by the carrier concentration and the activation energy changes associated with the incorporation of excess oxygen. © 1997 Academic Press

1. INTRODUCTION

Lanthanide nickel oxide $Ln_2NiO_{4+\delta}$ (Ln = a lanthanide element) is a K_2NiF_4-type compound (1). Although Sr substituted compounds, $Sm_{2-x}Sr_xNiO_{4\pm\delta}$ ($0.5 \leq x \leq 1.0$) and $GdSrNiO_4$, were prepared and their structural, electrical, and magnetic properties were investigated by Greenblatt *et al.* (2), $Sm_2NiO_{4+\delta}$, $Eu_2NiO_{4+\delta}$, and $Gd_2NiO_{4+\delta}$ have not been reported. Only three compounds are now obtained as $Ln_2NiO_{4+\delta}$ (Ln = La, Pr, or Nd). Discerning the trend in physical properties of $Ln_2NiO_{4+\delta}$ is difficult because some physical properties of $La_2NiO_{4+\delta}$, $Pr_2NiO_{4+\delta}$, and $Nd_2NiO_{4+\delta}$ are characteristic to each.

Phenomena commonly found in these three compounds are the existence of the metal–semiconductor transition (3–20) and excess oxygen (21–32), i.e., δ in $Ln_2NiO_{4+\delta}$. Much work has been reported about these phenomena. Ganguly and Rao studied the metallic behaviour of La_2NiO_4 and Nd_2NiO_4 above 500 K (3). The relationship between the electrical resistivities of La_2NiO_4 and $LaSrNiO_4$ and ambient oxygen was examined by the authors in a previous paper (8), where it was shown that the resistivities of La_2NiO_4 and $LaSrNiO_4$ are not oxygen pressure dependent below 581 K but decrease with increasing oxygen pressure above 673 K. Odier *et al.* presented very careful studies of the mass variations of $La_{2-x}NiO_{4+\delta}$ (30) and $Pr_2NiO_{4+\delta}$ (19) using a thermobalance. They pointed out that oxygen loss occurs in $La_{2-x}NiO_{4+\delta}$ and $Pr_2NiO_{4+\delta}$ above 600 K (19, 30) and concluded that the minimum of resistivity of $La_{2-x}NiO_{4+\delta}$ and $Pr_2NiO_{4+\delta}$ around 600 K is due to oxygen loss (19). A model of the metal–semiconductor transition of $La_{2-x}NiO_{4+\delta}$ was also proposed by them (16).

Figure 1 presents unpublished data. Powder of $La_2NiO_{4+\delta}$ (1.014 g) was loaded onto a Pt-boat which was put in an evacuated closed silica glass apparatus (3.5 dm^3). The pressure inside the apparatus was measured with a Pirani gauge up to 1373 K. This technique is called the preliminary desorption method. The data show that oxygen starts to desorb from $La_2NiO_{4+\delta}$ at 600 K and that desorption and absorption of oxygen are reversible above 750 K.

The previous (8) and present data (Fig. 1) indicate the importance of considering the variation of oxygen content in $La_2NiO_{4+\delta}$ in discussing the metal–semiconductor transition mechanism. However, the quality of the previous and the preliminary data was not good enough for discussing the mechanism, i.e., the relation between the oxygen variation and the electrical conductivity. The oxygen content of La_2NiO_4 was analyzed at room temperature (8) and the oxygen pressure was measured only in a low oxygen pressure region with the Pirani gauge in the present data (Fig. 1). Detection of oxygen variation *in situ* as a function of temperature and oxygen pressure is absolutely necessary, as Odier *et al.* had carried out with a thermobalance (16, 19, 30).

The purpose of this paper is to describe the effects of temperature and oxygen pressure on the excess oxygen concentration and electrical conductivity of $La_2NiO_{4+\delta}$, as determined *in situ* by a vacuum technique named the desorption method. The metal–semiconductor transition mechanism of $La_2NiO_{4+\delta}$ is examined using the *in situ* data. Although the metal–semiconductor transition is a common property of $Ln_2NiO_{4+\delta}$ (Ln = La, Pr, or Nd), only the properties of $La_2NiO_{4+\delta}$ will be examined in this paper, because some characteristic properties of $Pr_2NiO_{4+\delta}$ and $Nd_2NiO_{4+\delta}$ complicate the discussion for the transition mechanism: (i) While La in $La_2NiO_{4+\delta}$ and Nd in

[1] To whom correspondence should be addressed.

0022-4596/97 $25.00

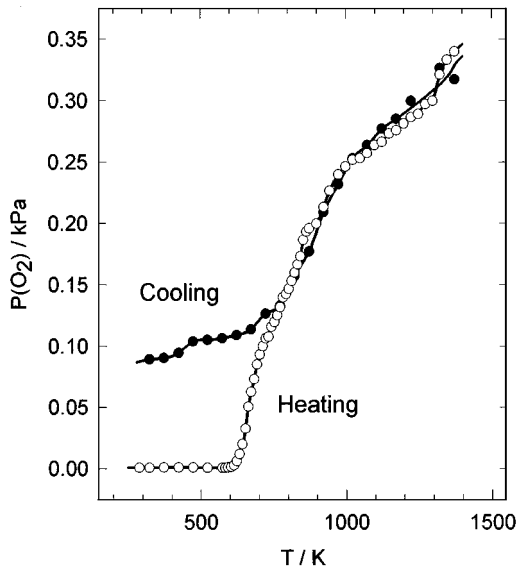

FIG. 1. Temperature dependence of oxygen pressure inside an evacuated silica glass apparatus (3.5 dm^3) up to 1373 K with a heating and cooling rate of 10 K min^{-1}. The oxygen was desorbed from and absorbed on $La_2NiO_{4+\delta}$ powder (1.014 g, $\delta = 0.111$ at 300 K) on a Pt boat in the vacuum apparatus. A Pirani gauge was used for the pressure measurements.

$Nd_2NiO_{4+\delta}$ exist as trivalent cations, a part of Pr in $Pr_2NiO_{4+\delta}$ may exist in the tetravalent state. Thus, the metal–semiconductor transition may be related to the Pr^{3+} and Pr^{4+} ratio in $Pr_2NiO_{4+\delta}$ which varies with temperature. (ii) The orthorhombic–tetragonal phase transition exists at 720 K for $Pr_2NiO_{4+\delta}$ (19) and at 848 K for $Nd_2NiO_{4+\delta}$ (14). The existence of the high-temperature structural phase transition may give rise to the metal–semiconductor transition. Thus, $La_2NiO_{4+\delta}$ may be the best candidate of the three compounds for examining the metal–semiconductor transition mechanism of $Ln_2NiO_{4+\delta}$.

Recently, Odier *et al.* found an anomaly in the resistivity curve of $Pr_2NiO_{4+\delta}$ at about 720 K at the orthorhombic–tetragonal phase transition temperature (19): the resistivity increases from 0.0415 to 0.0425 ohm cm with heating through the structural phase transition. This finding is important because it shows that the orthorhombic–tetragonal phase transition does not significantly change the shape of the resistivity curve and does not cause the metal–semiconductor transition for $Pr_2NiO_{4+\delta}$.

2. EXPERIMENTAL

$La_2NiO_{4+\delta}$ was prepared by heating the compressed powder of La_2O_3 (Nihon Yttrium, 99.9%) and NiO (Kojyundo Kagaku, 99.99%) at 1173 K for 24 h, at 1274 K for 24 h, and at 1423 K for 24 h, with intermittent grindings. The phase purity of the product was confirmed at room temperature with a Rigaku X-ray powder diffractometer RINT 1200 equipped with a Cu$K\alpha$ radiation source and a graphite monochromator. No secondary phase was detected in the diffraction pattern of $La_2NiO_{4+\delta}$.

The product was annealed in 101.33 $\pm$ 0.07 kPa of oxygen at 523 K for 18 h and was then quenched to room temperature. The excess oxygen concentration of the annealed and quenched oxide determined by iodometry was 0.1441 (standard deviation, 0.0038). The lattice constants of the successively quenched oxide were determined by the Rietveld program RIETAN (33, 34) with the structural model for $La_2NiO_{4+\delta}$ (orthorhombic *Fmmm*) proposed by Jorgensen *et al.* (22). The profile data were collected with the X-ray diffractometer RINT 1200 in air in the range 300–1200 K.

The excess oxygen concentrations of $La_2NiO_{4+\delta}$ at various temperatures and oxygen pressures were measured by the desorption method (Fig. 2). The $La_2NiO_{4+\delta}$ powder (4.2–9.8 g) was contained in a Pt crucible (PtC), which was suspended from a glass reel (GR) with a Pt wire (PtW), 0.2 mm in diameter, in a quartz tube (QT) (Fig. 2). The powder was annealed and quenched in the apparatus: the Pt crucible was put at the center of the furnace (F), heated (annealed) in 101.33 $\pm$ 0.07 kPa of oxygen at 523 K for 18 h, and pulled down to the bottom of the quartz tube (quenched to room temperature). The Pt crucible was kept at the bottom of the quartz tube until the temperature of the furnace reached the prescribed value (300–1273 K) and the oxygen pressure inside the quartz tube was regulated

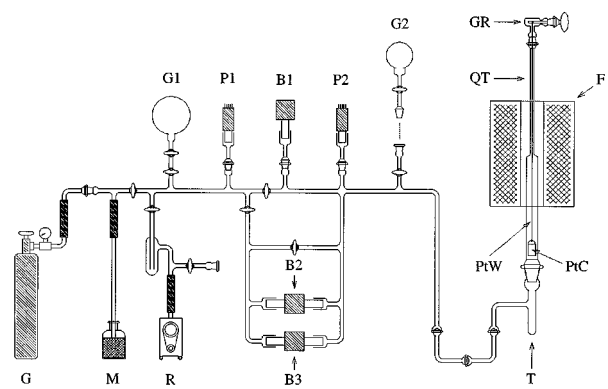

FIG. 2. Vacuum apparatus designed for determination of temperature and oxygen pressure dependencies of δ in $La_2NiO_{4+\delta}$. Electrical conductivities of $La_2NiO_{4+\delta}$ were also measured with the apparatus as functions of temperature and oxygen pressure in the ranges 300–1273 K and 0.1–71.4 kPa. B1, Baratron type 122A pressure gauge (0.0– + 1000.0 Torr); B2, Baratron type 223B pressure gauge (− 10.000– + 100.000 Torr); B3, Baratron type 223B pressure gauge (− 100.00– + 100.00 Torr) (1 Torr ≡ 133.32 Pa); F, furnace; G, gas cylinder; G1, gas balloon; G2, gas balloon (removable, 78.914 cm^3); GR, glass reel; P1, P2, Pirani gauge; PtC, Pt crucible; PtW, Pt wire (diameter, 0.2 mm); QT, quartz tube; R, rotary pump; T, trap; M, mercury column.

(the initial oxygen pressure: 0.00 ± 0.07, 13.33 ± 0.07, or 66.66 ± 0.07 kPa). The Pt crucible was pulled up to the center of the furnace, and the inside pressure of the quartz tube was recorded every 2 min with Baratron pressure gauges (B1, B2, and B3) until the reading was stabilized. This operation is named the desorption method.

The excess oxygen concentration of $La_2NiO_{4+\delta}$ at a given temperature and oxygen pressure is obtained from the pressure rise (the pressure difference between the initial and final oxygen pressures) and the apparent volume of the vacuum apparatus. The apparent volume of the vacuum apparatus was measured just after the final oxygen pressure measurements, because the apparent volume was altered by the furnace and the ambient temperatures, e.g., $365 \pm 2\,cm^3$ at the furnace temperature 373 K and $304 \pm 1\,cm^3$ at 1273 K. Boyle's law and a gas balloon (G2, $78.914\,cm^3$) were employed for the apparent volume measurements. The gas balloon, the volume of which was measured by Archimedes' method, was used as a volume standard during the apparent volume measurements.

The electrical conductivity of $La_2NiO_{4+\delta}$ was measured by the four probe technique in the temperature range 77.4–1273 K. The conductivity measurements below 300 K were performed on a sintered bar of $La_2NiO_{4+\delta}$ under an oxygen or helium gas atmosphere (1 atm). The sintered bar was annealed in 101.33 ± 0.07 kPa of oxygen at 523 K for 18 h and successively quenched to room temperature before the measurements.

The conductivity measurements above 300 K were carried out on a sintered pellet of $La_2NiO_{4+\delta}$ by the van der Pauw method (35, 36) with the vacuum apparatus in Fig. 2. The sintered pellet was annealed in 101.33 ± 0.07 kPa of oxygen at 523 K for 18 h prior to the conductivity measurements. The oxygen pressure inside the apparatus was set at 1.33 ± 0.07, 13.33 ± 0.07, 66.66 ± 0.07, or 101.33 ± 0.07 kPa at the annealing temperature of 523 K. The cooling process was selected for the conductivity measurements below 532 K and the heating process for those above 523 K.

3. RESULTS AND DISCUSSION

The lattice constants of the annealed and quenched sample of $La_2NiO_{4.1441}$ at 300 K are $a = 546.03(3)$ pm, $b = 546.31(3)$ pm, and $c = 1267.86(3)$ pm ($b - a = 0.25$ pm). Jorgensen *et al.* (22) reported the structure of $La_2NiO_{4.18}$ at 295 K (orthorhombic *Fmmm*) with the neutron powder diffraction data: $a = 546.14(2)$ pm, $b = 547.23(2)$ pm, and $c = 1271.38(2)$ pm ($b - a = 1.09$ pm). Mehta and Heaney (31) later reexamined the structure of $La_2NiO_{4.18}$ at 295 K (orthorhombic *Bbcm*) using the monochromatic synchrotron X-ray radiation: $a = 546.520(7)$ pm, $b = 546.869(7)$ pm, and $c = 1267.804(15)$ pm ($b - a = 0.349$ pm). The present values of the lattice constants are consistent with those reported by Mehta and Heaney. $La_2NiO_{4.1441}$ is assigned to be orthorhombic. However, the $(b - a)$ value of $La_2NiO_{4.1441}$ is only 0.25 pm and the (2 0 0) peak of $La_2NiO_{4.1441}$ is not at all split.

Freltoft *et al.* (24) reported on the orthorhombic–tetragonal phase transition of $La_2NiO_{4.065}$ at 232–240 K based on single crystal neutron diffraction data. The lattice constants of the orthorhombic phase at 9 K are $a = 545.2(2)$ pm, $b = 549.0(2)$ pm, and $c = 1261.7(2)$ pm ($b - a = 3.8$ pm). Tranquada *et al.* (32) also reported the orthorhombic–tetragonal phase transition of $La_2NiO_{4.105}$ at 285–290 K with the single crystal neutron diffraction data. The lattice constants of the orthorhombic phase at 280 K from their figure are $a = 545.5$ pm, $b = 550.5$ pm, and $c = 1265$ pm ($b - a = 5$ pm). Tranquada *et al.*, moreover, found a (2 0 0) peak splitting of $La_2NiO_{4.105}$ below the phase transition temperature. The (2 0 0) and (0 2 0) peaks began to appear after cooling to 290 K and waiting for several hours (32). The phase transition rate is very sluggish at 290 K.

The $(b - a)$ values of $La_2NiO_{4.065}$ (24) and $La_2NiO_{4.105}$ (32) below the respective phase transition temperatures, i.e., the orthorhombic phases (3–5 pm), are more than 10 times the present value (0.25 pm). Although the Rietveld refinement gives different values of a and b for $La_2NiO_{4.1441}$ (orthorhombic *Fmmm*) and each standard deviation of a and b (0.03 pm) is much smaller than the $(b - a)$ value (0.25 pm), the standard deviations are possibly underestimated in the calculation and $La_2NiO_{4.1441}$ is tetragonal (*I4/mmm*).

It is not an unusual experience in the ordinary experiment that an orthorhombic phase transforms to a tetragonal phase at a high temperature. High-temperature X-ray powder diffraction on $La_2NiO_{4+\delta}$ ($\delta = 0.1441$ at 300 K) up to 1200 K indicated no structural phase transition (Fig. 3).

Results of the excess oxygen concentration measurements for $La_2NiO_{4+\delta}$ are shown in Fig. 4. In the temperature range 300–550 K, the excess oxygen concentration does not change significantly with temperature and initial oxygen pressure. However, in the range 550–1273 K, the concentration decreased with increasing temperature and slightly increased with increasing initial oxygen pressure. The initiating temperature of the oxygen loss at around 570 K agrees well with the temperature of the resistivity minima of $La_2NiO_{4+\delta}$ reported by Odier *et al.* (16) and by us in this paper. The degree of the oxygen loss is suppressed by increasing the oxygen pressure, but the degree of the suppression is not very large under the experimental conditions (Fig. 4).

The influence of oxygen loss on the carrier concentration change of $La_2NiO_{4+\delta}$ is estimated by the relation

$$\Delta n(P_i, T_i, P_f, T_f) \equiv n(P_f, T_f) - n(P_i, T_i)$$

$$= 2 \times Z \times \{\delta(P_f, T_f) - \delta(P_i, T_i)\}/(a \times b \times c), \quad [1]$$

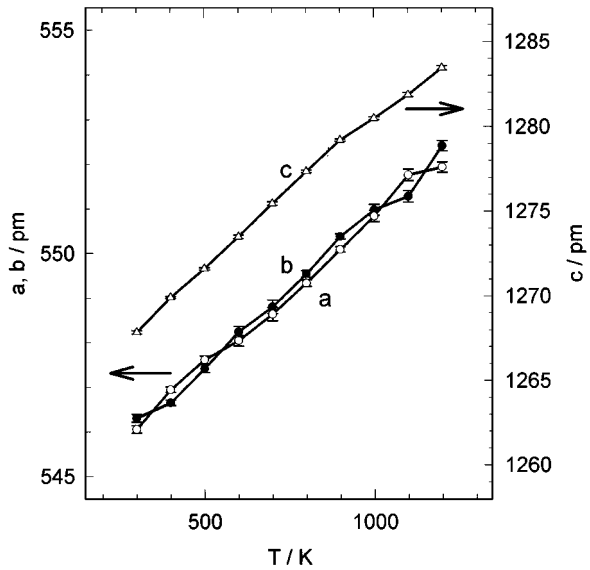

FIG. 3. Lattice constants of $La_2NiO_{4+\delta}$ ($\delta = 0.1441$ at 300 K) in air up to 1200 K. The error bars indicate 3σ (the standard deviation $\times 3$) of the lattice constants.

where $\Delta n(P_i, T_i, P_f, T_f)$ is the estimated carrier concentration change, the subscript i or f denotes the system in the initial or final state, $n(P_{i\,or\,f}, T_{i\,or\,f})$ the carrier concentration, $P_{i\,or\,f}$ the oxygen pressure, $T_{i\,or\,f}$ the temperature, Z the Z value of the unit cell of $La_2NiO_{4+\delta}$ ($Z = 4$), $\delta(P_{i\,or\,f}, T_{i\,or\,f})$ the excess oxygen concentration, and a, b, and c the lattice constants. The excess oxygen in the crystal is assumed to be in the bivalent state in the estimation. For an excess oxygen concentration of 0.1441 at 300 K and 0.0825 at 1273 K (Fig. 4), the estimated carrier concentration change becomes

$$\Delta n(P_i, 300\,\mathrm{K},\ P_f, 1273\,\mathrm{K}) \approx 1.3 \times 10^{21}\,\mathrm{cm}^{-3}. \qquad [2]$$

This value of $1.3 \times 10^{21}\,\mathrm{cm}^{-3}$ is large enough to give rise to a metal–semiconductor transition in most oxides.

The time required to achieve constant oxygen content decreases greatly with increasing temperature and somewhat with increasing oxygen pressure. This time is called settling time and is plotted on a log scale in Fig. 5. Note the sudden change of the settling time at about 600 K. This temperature also agrees with the resistivity minimum of $La_2NiO_{4+\delta}$ (16).

The electrical conductivity measurements for $La_2NiO_{4.1441}$ below 300 K are shown in Fig. 6. The $\log \sigma$ vs $T^{-1/4}$ plot in helium almost superimposes on the curve in oxygen. This phenomenon is consistent with the settling time measurements (Fig. 5). The $\log \sigma$ vs $T^{-1/4}$ plot, though not the Arrhenius plot, yields a good linear relationship for $La_2NiO_{4.1441}$ in the range 77.4–300 K (Fig. 6). Thus, the random-range hopping model is applicable to $La_2NiO_{4.1441}$ below 300 K (35, 37).

The electrical conductivity measurements for $La_2NiO_{4+\delta}$ above 300 K are shown in Fig. 7. The temperature dependence of the conductivity is divided into three regions: (i) In the range 300–410 K, $La_2NiO_{4+\delta}$ is a semiconductor. With increasing temperature, the conductivity curve changes from the random-range hopping type to the Arrhenius

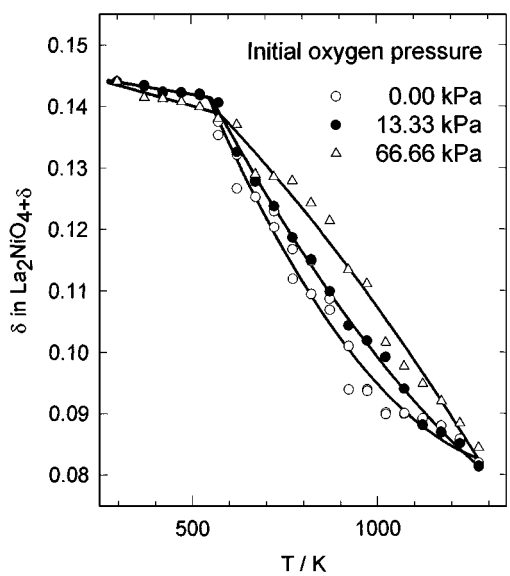

FIG. 4. Temperature dependence of the excess oxygen concentration δ in $La_2NiO_{4+\delta}$ ($\delta = 0.1441$ at 300 K) at the initial oxygen pressure 0.00, 13.33, or 66.66 kPa up to 1273 K.

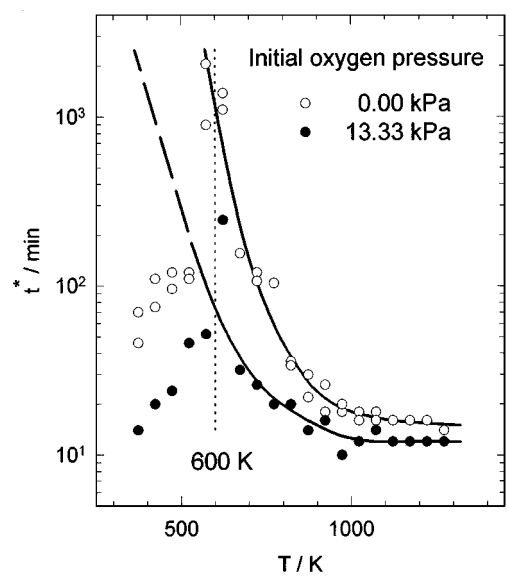

FIG. 5. Temperature dependence of the time required to settle the reading of oxygen pressure inside the vaccum apparatus in Fig. 2 (settling time t^*) for $La_2NiO_{4+\delta}$ ($\delta = 0.1441$ at 300 K) at the initial oxygen pressure 0.00 or 13.33 kPa in the range 373–1273 K.

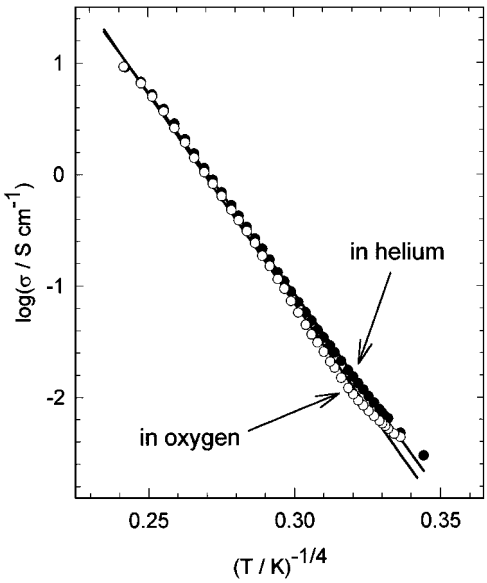

FIG. 6. Temperature dependence of the electrical conductivity of $La_2NiO_{4+\delta}$ ($\delta = 0.1441$ at 300 K) in the range 78–300 K under an oxygen or helium atmosphere (1 atm).

behavior. No oxygen pressure dependence is detected in the curves. (ii) In the range 410–550 K, $La_2NiO_{4+\delta}$ is an Arrhenius-type semiconductor. No oxygen pressure dependence is detected in this region either. (iii) In the range

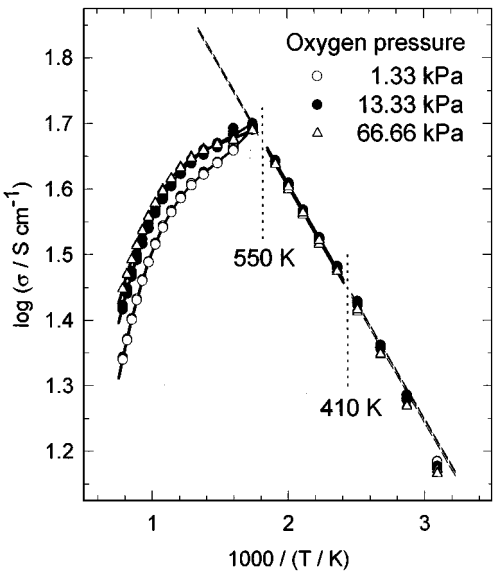

FIG. 7. Temperature dependence of the electrical conductivity of $La_2NiO_{4+\delta}$ ($\delta = 0.1441$ at 300 K) up to 1273 K in 1.33, 13.33, or 66.66 kPa of oxygen. The $La_2NiO_{4+\delta}$ sample was annealed in 101.33 ± 0.07 kPa of oxygen at 523 K for 18 h, and the conductivity measurements were successively continued from the annealing temperature of 523 down to 300 or up to 1273 K.

550–1273 K, $La_2NiO_{4+\delta}$ is a *p*-type metalic conductor, that is, the conductivity of $La_2NiO_{4+\delta}$ is decreased with increasing temperature and with decreasing oxygen pressure. The metal–semiconductor transition temperature is 573 K, close to the initiating temperature of the oxygen loss in Fig. 4 (570 K).

Three different models I, II, and III have been examined in explaining the metal–semiconductor transition mechanisms of $La_2NiO_{4+\delta}$. In the models, the following assumptions are included: (i) The stoichiometric compound La_2NiO_4 is an insulator (17, 20, 38). (ii) The nonstoichiometric compound $La_2NiO_{4+\delta}$ is a *p*-type extrinsic semiconductor. (iii) The oxide $La_2NiO_{4+\delta}$ is an Arrhenius-type semiconductor from 410 to 1273 K, provided the excess oxygen concentration does not change with temperature:

$$\sigma = n_0 e\mu \exp\{-E_a/(kT)\}. \quad [3]$$

(iv) The carrier concentration or the acceptor level concentration is directly proportional to the excess oxygen concentration,

$$n_0 = n_1\delta, \quad [4]$$

where n_1 is a constant.

Model I. It is assumed in the model that the metal–semiconductor transition is caused merely by the carrier concentration change owing to the excess oxygen concentration change (Eqs. [3] and [4]). The following relation must hold, if the model is correct:

$$\sigma/\delta = n_1 e\mu \exp\{-E_a/(kT)\}. \quad [5]$$

In plots of $\log(\sigma/\delta)$ vs $1/T$ the calculated conductivity curves are distinctly bent at 573 K, but not sufficiently to explain the metal–semiconductor transition of $La_2NiO_{4+\delta}$. The mobility or the activation energy change to temperature or oxygen pressure should be included in the model for explaining the metal–semiconductor transition of the compound.

Model II. In the second model, the metal–semiconductor transition is assumed to be caused by the carrier concentration change (Eq. [4]) and by the mobility change. The mobility is assumed to be

$$\mu = \mu_0/T, \quad [6]$$

where μ_0 is a constant. The mobility of a pure metal is assumed, because the mobility change with temperature should be large, if the transition is caused by carrier concentration and mobility changes. The following relation must hold, if the second model is correct:

$$\sigma T/\delta = n_1 e\mu_0 \exp\{-E_a/(kT)\}. \quad [7]$$

In plots of $\log(\sigma T/\delta)$ against $1/T$ the metal–semiconductor transition is not produced. The metal–semiconductor transition of $La_2NiO_{4+\delta}$ is explainable by the model, but the $\log(\sigma T/\delta)$ curves are still bent at 570 K; that is, the mobility change with temperature (Eq. [6]) is not large enough to explain the metal–semiconductor transition of $La_2NiO_{4+\delta}$. Furthermore, the mobility changes with temperature of most metallic compounds are not as large as those of a pure metal, because the residual resistivity of a compound is much larger than that of a pure metal. Applying the second model to the explanation of the metal–semiconductor transition of $La_2NiO_{4+\delta}$ is difficult.

Model III. In the third model, the metal–semiconductor transition is assumed to be caused by the carrier concentration change (Eq. [4]) and the activation energy change. The activation energy is assumed to be

$$E_a = E_0 + E_1\delta, \qquad [8]$$

where E_0 and E_1 are constants. The following relation must hold, if the third model is correct,

$$\sigma/\delta = n_1 e\mu \exp\{-(E_0 + E_1\delta)/(kT)\}, \qquad [9]$$

or

$$\log(\sigma/\delta) = A + B(1000/T) + C(1000\delta/T), \qquad [10]$$

$$A \equiv \log(n_1 e\mu),$$

$$B \equiv \{\log(e)/1000\}(-E_0/k),$$

$$C \equiv \{\log(e)/1000\}(-E_1/k),$$

where A, B, and C are the refinable parameters. A multiple linear regression is employed for evaluation of the parameters A, B, and C. The conductivity data in the range 300–1273 K (the raw data), the excess oxygen concentration data, and the statistical program SigmaStat (39) are used for the calculation.

The results of the regression are shown in Fig. 8. The values of E_0 and E_1 (Eq. [8]) are respectively positive and negative in the applicable oxygen pressure range. The agreement between the observed and the fitted values is very sensitive to the excess oxygen concentration data. The agreement is sufficient at the oxygen pressure 66.66 kPa, tolerable at 13.33 kPa, and not quite sufficient at 1.33 kPa (Fig. 8). The metal–semiconductor transition of $La_2NiO_{4+\delta}$ is basically explained by the third model. Despite the limited success of the present procedure, further investigations are necessary to clarify the true metal–semiconductor transition mechanism of $Ln_2NiO_{4+\delta}$.

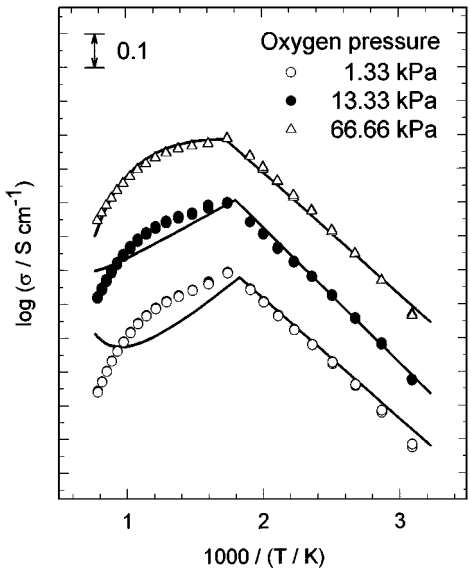

FIG. 8. Temperature dependence of the electrical conductivity of $La_2NiO_{4+\delta}$ ($\delta = 0.1441$ at 300 K) up to 1273 K in 1.33, 13.33, or 66.66 kPa of oxygen. The solid lines in the figure are the calculated conductivities of $La_2NiO_{4+\delta}$.

REFERENCES

1. A. Rabenau and P. Eckerlin, *Acta Crystallogr.* **11,** 304 (1958).
2. S. C. Chen, K. V. Ramanujachary, and M. Greenblatt, *J. Solid State Chem.* **105,** 444 (1993).
3. P. Ganguly and C. N. R. Rao, *Mater. Res. Bull.* **8,** 405 (1973).
4. C. P. Tavares, *Mater. Res. Bull.* **20,** 979 (1985).
5. D. J. Buttrey, J. M. Honig, and C. N. R. Rao, *J. Solid State Chem.* **64,** 287 (1986).
6. K. Ishikawa, S. Kondo, Y. Suzuki, S. Takayama K. Shimada, and Y. Suzuki, *Bull. Chem. Soc. Jpn.* **59,** 703 (1986).
7. M. Sayer and P. Odier, *J. Solid State Chem.* **67,** 26 (1987).
8. K. Ishikawa, S. Kondo, H. Okano, S. Suzuki, and Y. Suzuki, *Bull. Chem. Soc. Jpn.* **60,** 1295 (1987).
9. K. Dembinski, J. M. Bassat, J. P. Coutures, and P. Odier, *J. Mater. Sci. Lett.* **6,** 1365 (1987).
10. Z. Kakol, J. Spałek, and J. M. Honig, *J. Solid State Chem.* **79,** 288 (1989).
11. J. M. Bassat, F. Gervais, P. Odier, and J. P. Loup, *Mater. Sci. Eng. B.* **3,** 507 (1989).
12. B. W. Arbuckle, K. V. Ramanujachary, Z. Zhang, and M. Greenblatt, *J. Solid State Chem.* **88,** 278 (1990).
13. Y. Takeda, M. Nishijima, N. Imanishi, R. Kanno, O. Yamamoto, and M. Takano, *J. Solid State Chem.* **96,** 72 (1992).
14. B. W. Arbuckle, K. V. Ramanujachary, A. M. Buckley, and M. Greenblatt, *J. Solid State Chem.* **97,** 274 (1992).
15. X. Granados, J. Fontcuberta, M. Vallet-Regí, M. J. Sayagués, and J. M. Gonzáles-Calbet, *J. Solid State Chem.* **102,** 455 (1993).
16. J. M. Bassat, P. Odier, and J. P. Loup, *J. Solid State Chem.* **110,** 124 (1994).
17. K. Sreedhar, M. McElfresh, D. Perry, D. Kim, P. Metcalf, and J. M. Honig, *J. Solid State Chem.* **110,** 208 (1994).
18. K. Sreedhar and J. M. Honig, *J. Solid State Chem.* **111,** 147 (1994).
19. C. Allançon, A. Gonthier-Vassal, J. M. Bassat, J. P. Loup and P. Odier, *Solid State Ionics* **74,** 239 (1994).
20. Z. Zhang and M. Greenblatt, *J. Solid State Chem.* **117,** 236 (1995).
21. J. Rodríguez-Carvajal, J. L. Martínez, J. Pannetier, and R. Saez-Puche, *Phys. Rev. B* **38,** 7148 (1988).

22. J. D. Jorgensen, B. Dabrowski, S. Pei, D. R. Richards, and D. G. Hinks, *Phys. Rev. B* **40,** 2187 (1989).
23. G. H. Lander, P. J. Brown, J. Spałek and J. M. Honig, *Phys. Rev. B* **40,** 4463 (1989).
24. T. Freltoft, D. J. Buttrey, G. Aeppli, D. Vaknin, and G. Shirane, *Phys. Rev. B* **44,** 5046 (1991).
25. L. C. Otero-Diaz, A. R. Landa, F. Fernandez, R. Saez-Puche, R. Withers, and B. G. Hyde, *J. Solid State Chem.* **97,** 443 (1992).
26. D. E. Rice and D. J. Buttrey, *J. Solid State Chem.* **105,** 197 (1993).
27. A. Demourgues, A. Wattiaux, J. C. Grenier, M. Pouchard, J. L. Soubeyroux, J. M. Dance, and P. Hagenmuller, *J. Solid State Chem.* **105,** 458 (1993).
28. A. Demourgues, F. Weill, B. Darriet, A. Wattiaux, J. C. Grenier, P. Gravereau, and M. Pouchard, *J. Solid State Chem.* **106,** 317 (1993).
29. A. Demourgues, F. Weill, B. Darriet, A. Wattiaux, J. C. Grenier, P. Gravereau, and M. Pouchard, *J. Solid State Chem.* **106,** 330 (1993).
30. P. Odier, J. M. Bassat, J. C. Rifflet, and J. P. Loup, *Solid State Commun.* **85,** 561 (1993).
31. A. Mehta and P. J. Heaney, *Phys. Rev. B* **49,** 563 (1994).
32. J. M. Tranquada, Y. Kong, J. E. Lorenzo, D. J. Buttrey, D. E. Rice, and V. Sachan, *Phys. Rev. B* **50,** 6340 (1994).
33. F. Izumi, "The Rietveld Method" (R. A. Young, Ed.), Chap. 13. Oxford Univ. Press, Oxford, 1995.
34. Y. I. Kim and F. Izumi, *J. Ceram. Soc. Jpn.* **102,** 401 (1994).
35. A. Hamnett, "Solid State Chemistry: Techniques" (A. K. Cheetham and P. Day, Eds.), Chap. 8. Oxford Univ. Press, Oxford, 1988.
36. L. J. van der Pauw, *Philips Res. Rep.* **13,** 1 (1958).
37. N. F. Mott, *Phil. Mag.* **19,** 835 (1967).
38. K. K. Singh, P. Ganguly, and J. B. Goodenough, *J. Solid State Chem.* **52,** 254 (1984).
39. Jandel Scientific, "SigmaStat for Windows Version 1.0; User's Manual."